Air Bubble Entrainment, Breakup, and Interplay in Vertical Plunging Jets

Numa Bertola[1]
School of Civil Engineering,
The University of Queensland,
Brisbane QLD 4072, Australia

Hang Wang[2]
School of Civil Engineering,
The University of Queensland,
Brisbane QLD 4072, Australia
e-mail: hang.wang@uqconnect.edu.au

Hubert Chanson
School of Civil Engineering,
The University of Queensland,
Brisbane QLD 4072, Australia

The entrainment, breakup, and interplay of air bubbles were observed in a vertical, two-dimensional supported jet at low impact velocities. Ultra-high-speed movies were analyzed both qualitatively and quantitatively. The onset velocity of bubble entrainment was between 0.9 and 1.1 m/s. Most bubbles were entrained as detached bubbles from elongated air cavities at the impingement point. Explosion, stretching, and dejection mechanisms were observed for individual bubble breakup, and the bubble interaction behaviors encompassed bubble rebound, "kiss-and-go," coalescence and breakup induced by approaching bubble(s). The effects of jet impact velocity on the bubble behaviors were investigated for impact velocities from 1.0 to 1.36 m/s, in the presence of a shear flow environment. [DOI: 10.1115/1.4039715]

1 Introduction

A plunging jet is a rapid liquid jet plunging into a relatively slow body of the same or a different fluid. The near-field flow region downstream of the impingement point is a turbulent shear flow, with transfer of momentum from the impinging flow to the surrounding bath. The plunging jet flow pattern varies for different jet impact velocities [1]. For a water jet with free surface open to atmosphere, air entrainment takes place at the impingement point when the jet impact velocity exceeds a critical onset velocity V_e [2–4]. The entrained air bubbles affect significantly the characteristics of the downstream shear flow by air–water mixing and bubble–turbulence interplay. For example, the plunging pool is highly aerated at large impact velocities, leading to unsteady flow bulking, bubble grouping during advection, and modification of turbulence field [5]. On the other hand, when the impact velocity is relatively small and slightly greater than V_e, particle interplay is primarily limited among a small number of neighboring bubbles, in the absence of large-scale turbulent structures in surrounding water [3]. The bubble behavior, including their entrainment, breakup and interplay/coalescence, is directly related to the interfacial area in mass and heat transfer in the two-phase flow, thus is important in many industrial applications [6,7]. The presence of large eddy structures and turbulent shear forces in a plunging jet can further complicate the bubble motions, deformation, and dynamics.

Air entrainment in plunging jets is a process sensitive to both impact velocity and turbulence level in the impinging jet [4,8]. For given fluid properties (e.g., viscosity, surface tension), the occurrence of bubble breakup in a homogeneous turbulent flow is related to the interfacial oscillations induced by the flow velocity fluctuations and the response of surface tension [9–11]. The effects of gravity, shear stress, inhomogeneous turbulence, and any form of flow instabilities may add to nonzero average bubble deformation [12]. A relevant parameter to the bubble coalescence is the relative bubble approach velocity [13]. In applications like plunging jet, approach velocity observations implied an instant coalescence regime with typical coalescence time smaller than 10^{-2} s [14]. There have been vast amount of analytical, physical, and numerical studies of bubble breakup and coalescence, most of which focused on artificially generated bubbles in well-controlled turbulent environment [15–18]. Fewer studies were dedicated to self-aerated flows like circular and planar plunging jets with in-depth description of the air-phase behavior. One of the bottlenecks of the research is the inadequate measuring techniques, and the lack of physical information hampers the progress in numerical simulation investigation when the coalescence and breakup models need experimental guidance and verification [6].

The aim of this work is to present a statistical description of bubble behavior in self-aerated plunging jets at relatively low impact velocities. Observation of self-entrained individual bubbles or bubble clusters was performed using high-speed camera visualization at flow conditions close to the onset of air entrainment, and the images were analyzed qualitatively and quantitatively.

2 Experimental Setup

A two-dimensional planar water jet was issued from a 0.269 m wide rectangular nozzle with a 0.012 m nozzle opening. The planar jet was supported by a full-width polyvinyl chloride sheet extending from the nozzle edge into the receiving pool. The jet support was set at 88.5 deg to the horizontal to prevent flow detachment. It was built with lateral transparent window to facilitate flow visualization. The receiving tank was a 2.5 m long, 1 m wide, 1.5 m deep, in which the bath water level was controlled with a sharp-crested weir. The deep pool setup ensured that the bottom had no effect on the air entrainment and diffusion process in upper part of the pool.

Brisbane tap water was supplied from a constant head tank and the water discharge was measured with an orifice meter installed in the supply pipelines and calibrated on-site. Observations of bubble behavior were carried out using a Phantom Ultra-high-speed digital camera (v2011) equipped with a Carl Zeiss Planar T*85 mm f/1.4 lens, producing images with an absolutely negligible degree (~0.1%) of barrel distortion. The camera system was able to record up to 22,000 monochrome frames per second in high definition (1280 × 800 pixels, pixel size 28 μm) or 1,000,000 frames per second in low definition (128 × 16 pixels). Herein, the recording was set between 600 fps and 10,000 fps in high definition, and the total number of recorded frames was 33,285 frames, independently of the frame rate. The video movies were analyzed manually to guarantee maximum reliability of the data. The camera was positioned beside the plunge pool. The observation window was 10 cm wide and 20 cm long, while the depth of field was less than 20 mm. The observations were two-dimensional, and

[1]Present address: ETH-Zürich, Future Cities Laboratory, Singapore 138602.
[2]Corresponding author.

Contributed by the Fluids Engineering Division of ASME for publication in the Journal of Fluids Engineering. Manuscript received October 2, 2017; final manuscript received March 16, 2018; published online May 2, 2018. Assoc. Editor: Matevz Dular.

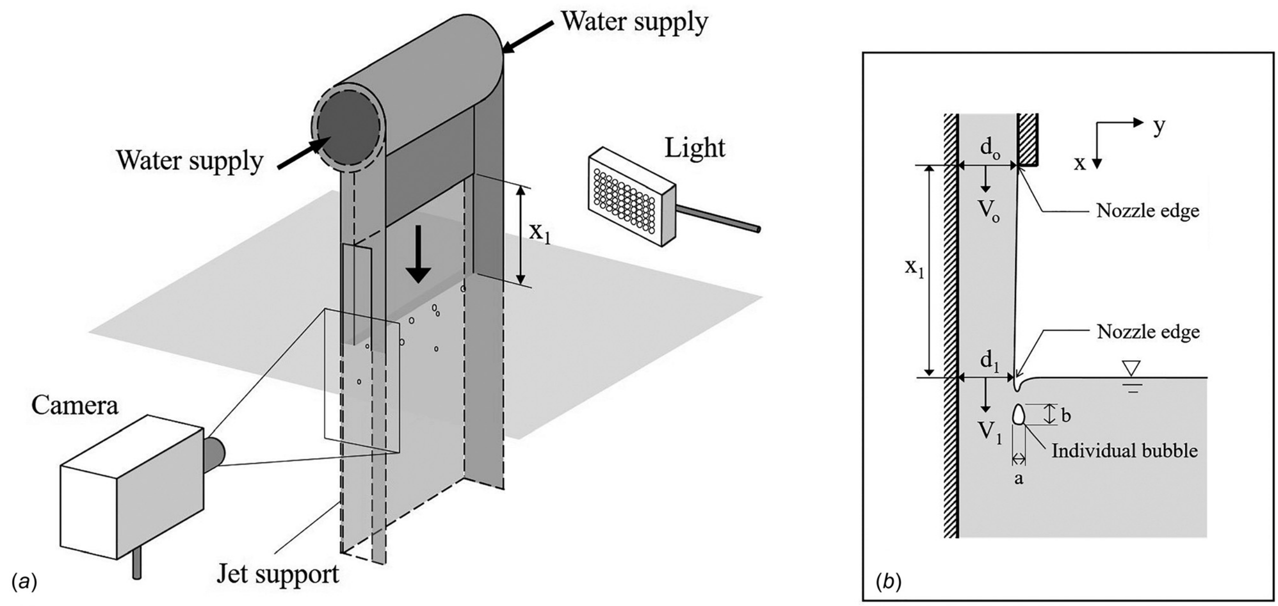

Fig. 1 Sketches of experimental setup: (*a*) relative position of jet nozzle and camera system and (*b*) side view of jet impingement and definition of relevant parameters

Table 1 Onset velocity of air bubble entrainment at vertical supported jet

Increasing discharge				Decreasing discharge			
Q (m^3/s)	x_1 (m)	V_e (m/s)	We_e	Q (m^3/s)	x_1 (m)	V_e (m/s)	We_e
0.0021	0.042	1.12	119	0.0023	0.018	0.92	107
0.0022	0.022	0.94	105	0.0022	0.018	0.90	100
0.0023	0.018	0.92	107	0.0021	0.020	0.90	96

Note: V_e—jet impact velocity, We_e—onset Weber number defined as $\mathrm{We}_e = \rho_w V_e^2 d_1/\sigma$.

three-dimensional patterns could not be recorded. Figure 1(*a*) shows a sketch of the relative positions of the experimental facility and high-speed camera system. A detailed side-view sketch of jet impingement is demonstrated in Fig. 1(*b*), along with definitions of relevant parameters.

The observations of individual bubble entrainment, breakup, and coalescence were conducted with water discharges $Q = 0.0021$–0.003 m^3/s and jet lengths $x_1 = 0.018$–0.05 m, yielding a range of jet impact velocities $V_1 = 0.90$–1.36 m/s. Further observations of vertical impingement point oscillations and downstream ejection of bubbly vortical structures were carried out for larger discharges $Q = 0.012$–0.04 m^3/s and jet lengths $x_1 = 0.1$–0.35 m, corresponding to impact velocities $V_1 = 1.87$–4.35 m/s.

3 Air Entrainment Onset Velocity

The onset of air bubble entrainment was defined as a primary entrainment event which is observed less than an interval of 5 min, following [3]. Herein, each experiment was conducted twice, first with increasing discharge and second with decreasing discharge approaching the onset of air entrainment, because the air bubble inception process showed some hysteresis. This is illustrated in Table 1, showing a larger onset velocity with increasing flow rate. The hysteresis was likely caused by some free-surface instability. The onset velocity V_e, namely, the jet impact velocity V_1 for the onset of bubble entrainment conditions, was determined for three discharges $Q = 0.0021$, 0.0022, and 0.0023 m^3/s. For $Q < 0.0021$ m^3/s, the jet flow rate was unstable and air could enter

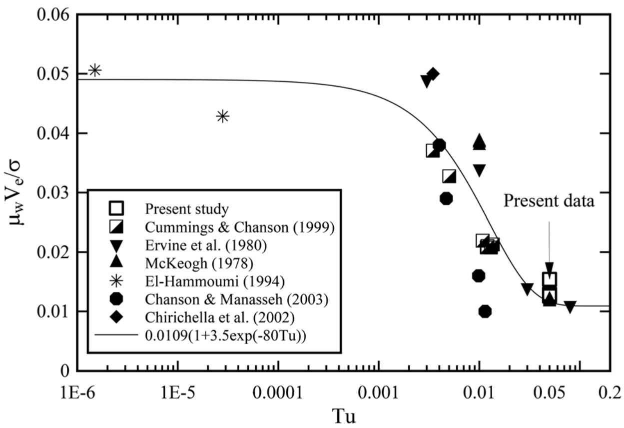

Fig. 2 Dimensionless onset velocity $\mu_w V_e/\sigma$ as a function of the jet turbulence intensity $\mathrm{Tu} = v'/V$, with comparison to past planar jet results [3] and circular jet results [8,19,21–23]

into the nozzle. For $Q > 0.0023$ m^3/s, the initial velocity at the nozzle was larger than the onset velocity. The results are summarized in Table 1, showing the onset velocity as a function of the water discharge and jet length for both series of observations.

Herein, the inception velocity results are discussed in terms of the increasing discharge data set only, in line with earlier studies [3,19]. The observations indicated onset velocities of air entrainment ranging from $V_e = 0.9$ to 1.1 m/s for jet lengths between $x_1 = 0.018$ and 0.042 m. Such onset conditions corresponded to a critical Weber number $\mathrm{We}_e \sim 100$–120, close to the findings of Refs. [3] and [20] but smaller than a minimum air-entrainment Weber number $\mathrm{We}_e = 400$ proposed for short turbulent circular jets [4]. The present results are compared to previous studies in Fig. 2, where the dimensionless onset velocity is presented as a function of the jet turbulence. Herein, the jet turbulence intensity was approximated to be 5% based upon total pressure measurements. Despite differences in definitions of air entrainment onset and of turbulence intensity, the experimental results showed a consistent trend. That is, the onset velocity decreases with increasing jet turbulence level. At the limits, $V_e \sim 3.5$ m/s for very-low

Table 2 Experimental observations of different air bubble entrainment mechanisms at a vertical plunging jet

V_1 (m/s)	x_1 (m)	Q (m^3/s)	Investigation duration (s)	Total number of entrained bubbles	Entrainment rate (Hz)	Number of individual entrapped bubbles	Number of elongated air cavity bubbles	Number of pre-entrained bubbles	Number of re-entrained bubbles
1.00	0.02	0.0025	11.9	88	7.4	15	37	23	13
1.12	0.02	0.0030	6.66	218	32.7	39	131	35	13
1.26	0.05	0.0025	3.33	165	49.5	12	135	9	9
1.36	0.05	0.0030	3.33	249	74.8	17	212	16	4

turbulence and $V_e \sim 0.8$ m/s for rough turbulent jets. Overall, the entire data set followed relatively closely:

$$\frac{\mu_w V_e}{\sigma} = 0.0109\left(1 + 3.5e^{-80\mathrm{Tu}}\right) \quad (1)$$

where μ_w is the water dynamic viscosity, σ is the surface tension between air and water, and Tu is the jet turbulence intensity, with a standard error of 0.0072 and a normalized correlation coefficient of 0.84. First introduced for two-dimensional vertical plunging jets [3], Eq. (1) encompasses both vertical two-dimensional and circular jet data, as seen in Fig. 2.

4 Mechanisms of Air Bubble Entrainment

When the impact velocity is larger than the onset velocity ($V_1 > V_e$), air bubbles are entrained at the impingement point between the supported free-falling jet and the pool of still water. The mechanisms of air bubble entrainment differ depending on the jet impact velocities [3]. Herein, the analysis of ultra-high-speed high-definition movies was performed for low impact velocities slightly greater than the onset velocity, i.e., $V_1 = 1.00$, 1.12, 1.26, and 1.36 m/s (Table 2). For these flow conditions, the results highlighted that the entrained bubble count rate F increased almost linearly with increasing jet impact velocity

$$\frac{F\,d_1}{V_1} = 0.167\frac{V_1}{\sqrt{g\,d_1}} - 0.407 \quad \text{for } 1.0\,\text{m/s} < V_1 < 1.36\,\text{m/s} \quad (2)$$

Four main mechanisms of air entrainment were observed: (a) single bubble entrapment, (b) breakup of an elongated air cavity, (c) pre-entrainment of air bubbles in the jet, and (d) bubble re-entrainment in the pool. They are presented below, followed by a discussion of the influence of the jet impact velocity.

The first bubble entrainment mechanism was the entrapment of a single air bubble at the impingement point. The individual bubble entrapment took place almost randomly along the impingement perimeter, and was likely associated with the formation of an air layer next to the jet free surface that intruded into the receiving water at the jet–pool intersection. The proportion of individual bubble entrapment decreased with increasing jet impact velocity. The observations are reported in Table 2. This mechanism became infrequent for larger impact velocities with a proportion of 7% for $V_1 = 1.36$ m/s.

The second bubble entrainment mechanism was the formation of an elongated air cavity at the impinging point and its subsequent breakup. An almost one-dimensional air finger was stretched, before its extremity was pinched off and broken into a single or multiple bubbles (Fig. 3). The upper part of the air finger was not entrained and would rise up to the free surface. Only the lower part of the air cavity could be considered as entrained air bubble(s). The overall process tended to take place in three successive phases as illustrated in Fig. 3: (1) the development of the air cavity (Figs. 3(*a*)–3(*c*)), (2) the stretching of the air cavity (Figs. 3(*d*)–3(*f*)), and (3) the cavity pinch-off, air pocket formation and breakup (Figs. 3(*g*)–3(*i*)). In Fig. 3, the entire process took place in less than 40 ms. Herein, the proportion of bubbles detached from elongated air cavities increased with increasing jet impact velocity (Table 2). The elongated air cavity mechanism was the most common bubble entrainment mechanism at larger impact velocities. For example, the proportion of entrained bubbles was 85% for an impact velocity $V_1 = 1.36$ m/s. For larger impact velocities, this mechanism could be considered as the dominant entrainment mechanism.

The third bubble entrainment mechanism was some pre-aeration bubbles coming from the supported free-falling jet. These bubbles were entrained above the impinging line. Some bubbles were entrained along the free surface of the supported free-falling jet. Other bubbles might have been entrained upstream of the nozzle as a result of air entering into the supply pipe at very low discharges. Quantitatively, the proportion of pre-entrained air bubbles tended to decrease with increasing impact velocity (Table 2).

The last mechanism was the re-entrainment of a rising bubble. With this mechanism, a detrained bubble rose up to the free surface of the pool where it stayed at the water surface and drifted slowly toward the impinging perimeter. Eventually, the bubble was re-entrained. Overall, the proportion of re-entrained bubbles decreased with increasing impact velocity (Table 2). This mechanism was the least likely for 1 m/s $< V_1 <$ 1.36 m/s. However, for larger impact velocity in presence of large-scale vortical structures, the re-entrainment of rising bubbles was noticeable. A large number of bubbles accumulated in a foamy layer at the free surface of the pool and many were driven back into the pool by the shear flow. More bubbles were re-entrained into the shear layer before they reached the free-surface by the recirculating motion of large vortices in which they were advected.

Figure 4 compares the respective proportion of bubble entrainment mechanisms as a function of the dimensionless impact velocity, showing the air-cavity breakup mechanism being the dominant mechanism with an increasing proportion with increasing jet impact velocity. The observation results were only valid for small impact velocities with minimum flow instabilities and absence of large vortices.

Observations at higher impact velocities further showed the importance of jet disturbance affecting the air entrainment mechanisms. Figure 5 sketches the effects of jet disturbance levels on the induction of single air bubbles or elongated air cavities. The first and second bubble entrainment mechanisms mentioned above are illustrated, respectively, for low and high jet disturbances. The pinch-off of air finger/elongated cavity in Fig. 5(*b*) was observed to be affected by a combination of several physical processes: (a) surrounding pressure exerted on the entrained air finger perimeter that overcame the capillary force as the finger elongated and surface curvature enlarged, (b) shear stress between the impinging flow and still plunge pool water that stretched and deformed the air cavity, (c) secondary helicoidal current forming around the finger itself, similar to a whirlpool with a streamwise axis, that twisted the finger, and (d) unsteady flow recirculation induced by flow bulking and large-scale vortices, which induced instability of the flow field in the vicinity of impingement point.

5 Individual Bubble Entrainment and Breakup

The behavior of individual entrained bubbles was investigated in details for three impact velocities slightly larger than the onset velocity, i.e., $V_1 = 1.00$ m/s, 1.12 m/s, and 1.26 m/s. Four different air bubble entrainment behaviors were observed: (a) no-

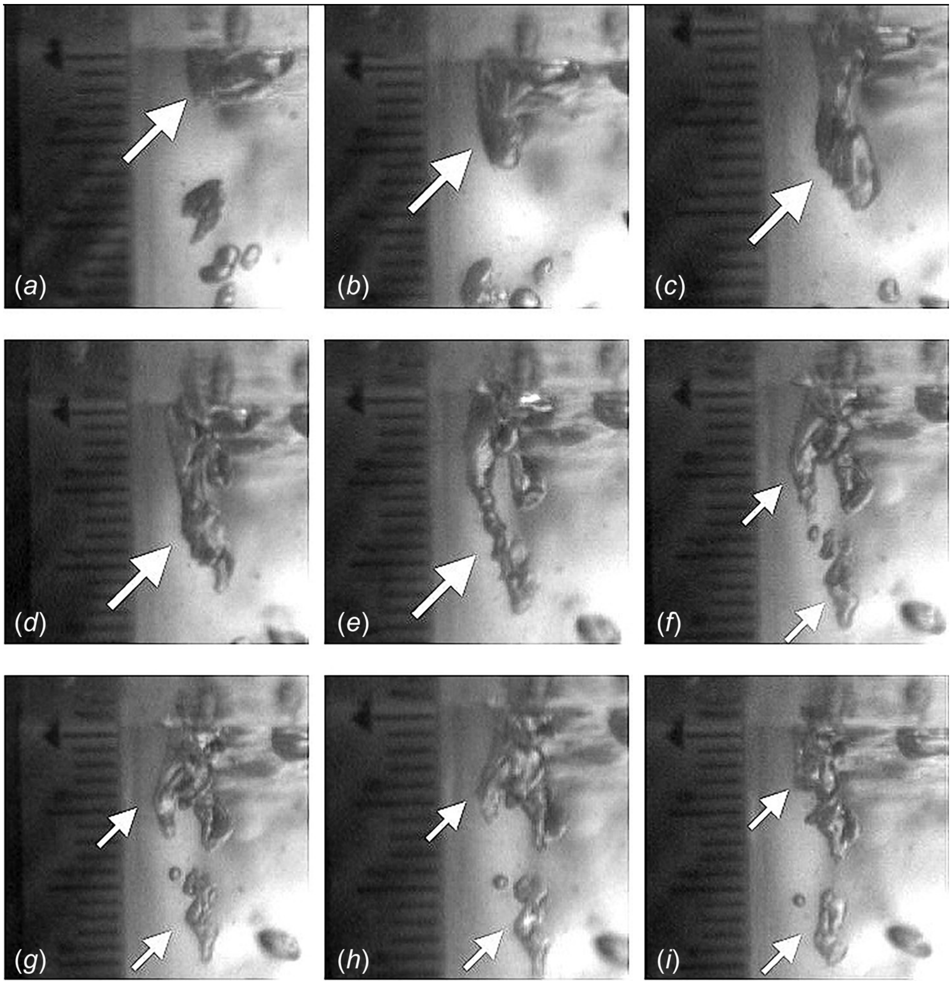

Fig. 3 Photographic sequence of the formation and breakup of an elongated air cavity at a plunging jet. Flow conditions: $V_1 = 1.26$ m/s, $x_1 = 0.05$ m. (1) Development of the air cavity: (*a*) $t = 0.000$ s, (*b*) $t = 0.012$ s, and (*c*) $t = 0.023$ s. (2) Stretching of the air cavity: (*d*) $t = 0.028$ s, (*e*) $t = 0.033$ s, and (*f*) $t = 0.035$ s. (3) Cavity pinch-off, air pocket formation and breakup: (*g*) $t = 0.036$ s, (*h*) $t = 0.038$ s, and (*i*) $t = 0.040$ s. Arrows indicating entrained air cavity and bubble(s).

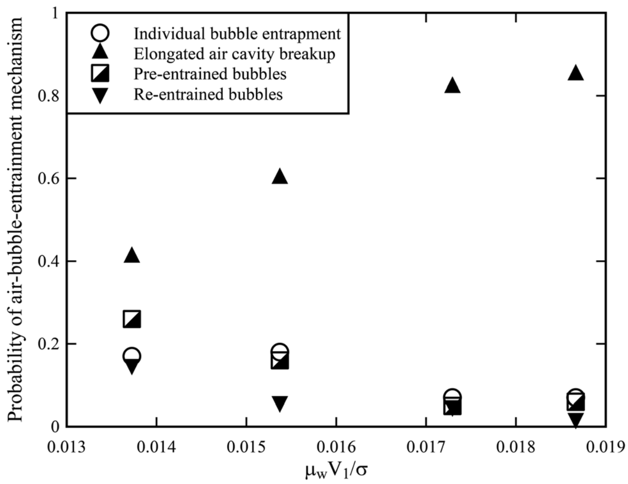

Fig. 4 Proportion of air entrainment mechanisms as functions of the impact velocity V_1 in a vertical supported plunging jet

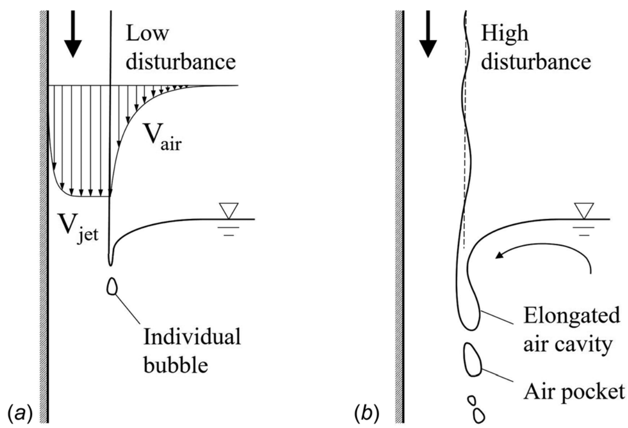

Fig. 5 Sketch of typical air entrainment mechanisms for low disturbance jet (*a*) and high disturbance jet (*b*)

interaction behavior where the bubble had almost no interaction and experienced no major modification during the air–water flow motion, (b) rising-up behavior where the bubble went back and rose up to the free surface, (c) breakup behavior where the bubble became unstable and broke into daughter bubbles, and (d) bubble interplay and coalescence behavior characterized by interactions of multiple parent bubbles and formation of a larger but often unstable bubble in the case of coalescence. The breakup behavior is discussed in this section, and the interaction behavior is presented in Sec. 6 as it is not considered as an individual bubble behavior.

The individual bubble entrainment properties were tracked for one impact velocity $V_1 = 1.00$ m/s. A total of 88 bubbles were entrained during 11.9 s observation timespan, corresponding in average to an occurrence of bubble entrainment in every 0.15 s. The big air packets that came certainly from a partially filled pipe were not taken into account in this study. The average distance between two successive bubbles was about $\Delta x = 0.069$ m. Since the distance between the bubbles was much larger than the average bubble size at the entrapment point (see below), most bubbles exhibited an individual bubble behavior. The average longitudinal bubble velocity V_b was derived from the total vertical distance covered by the bubble during its lifetime. The average bubble velocity was smaller than the inflow velocity, the ratio being $V_b/V_1 \sim 0.46$. Typically, the bubble was decelerated once it was entrained away from the impingement point. The bubble path was not perfectly vertical during all its lifetime. Denoting a and b as the median bubble dimensions in the longitudinal and normal directions, respectively (Fig. 1(*b*)), a and b were almost identical at the impingement point, i.e., $a = 3.49$ mm and $b = 3.47$ mm. Thus, the two-dimensional projection of bubble shape was almost circular at the entrapment point. Below the impingement point, the normal bubble dimension decreased, and the bubble shape became slightly flatter with increasing longitudinal distance, with $a = 3.63$ mm and $b = 3.25$ mm at 0.2 m below the pool free surface. In terms of different bubble behaviors for $V_1 = 1.0$ m/s, most individual bubbles presented a no-interaction behavior (75%) or a breakup behavior (10%). The proportions of rising-up and interplay behaviors were 8% and 6%, respectively.

The number of observed primary individual bubble breakup events was relatively small, i.e., nine breakups for $V_1 = 1.0$ m/s during 11.9 s, 37 breakups for $V_1 = 1.12$ m/s during 6.66 s, and 24 breakups for $V_1 = 1.26$ m/s during 3.33 s. These corresponded to 10–17% of the total entrained bubbles. Here, the bubble prior to breakup is called the mother bubble. The bubbles resulting from a breakup are called daughter bubbles. Following the initial breakup, called primary breakup, a number of daughter bubbles also experienced secondary breakups. Three main breakup mechanisms were observed: (a) explosion mechanism, (b) stretching mechanism, and (c) small dejection mechanism. For the explosion mechanism, the breakup appeared without any particular split point (Fig. 6). The explosive breakup process consisted usually of three steps: the apparition of bubble "instabilities" induced by ambient eddies with sufficient turbulent energy, the explosion of the unstable mother bubble, and the formation of daughter bubbles. The mother bubbles were usually larger than for the other breakup mechanisms, and they had not a stable shape. The number of daughters could be greater than two. Figure 6 shows an example of a mother bubble with an explosive mechanism breaking up into multiple daughter bubbles.

The second breakup mechanism was the stretching mechanism. Figure 7 illustrates an example: the mother bubble was stretched, until it broke into independent daughters with different behaviors. Usually, the number of daughter bubbles was equal to two, as seen in Fig. 7.

The third breakup mechanism was the small dejection mechanism (Fig. 8). In the example shown in Fig. 8, the mother bubble was first stretched, as in the precedent (stretching) mechanism, but the first dejection resulted in a mother bubble and daughter bubble(s) of significantly different sizes. The mother and daughter bubbles often showed independent behaviors, sometimes followed by a second dejection (Fig. 8(*g*)) and so on. This process could be repeated more than once.

Figure 9 shows some quantitative properties of bubble breakup events as functions of the impact velocity. The dimensionless occurrence frequency of bubble breakup $\sigma F_{break}/(\mu_w g)$, as well as the proportion of entrained bubbles experiencing a (primary) breakup, increased with increasing dimensionless impact velocity $\mu_w V_1/\sigma$ (Fig. 9(*a*)). Overall, the proportion of each breakup

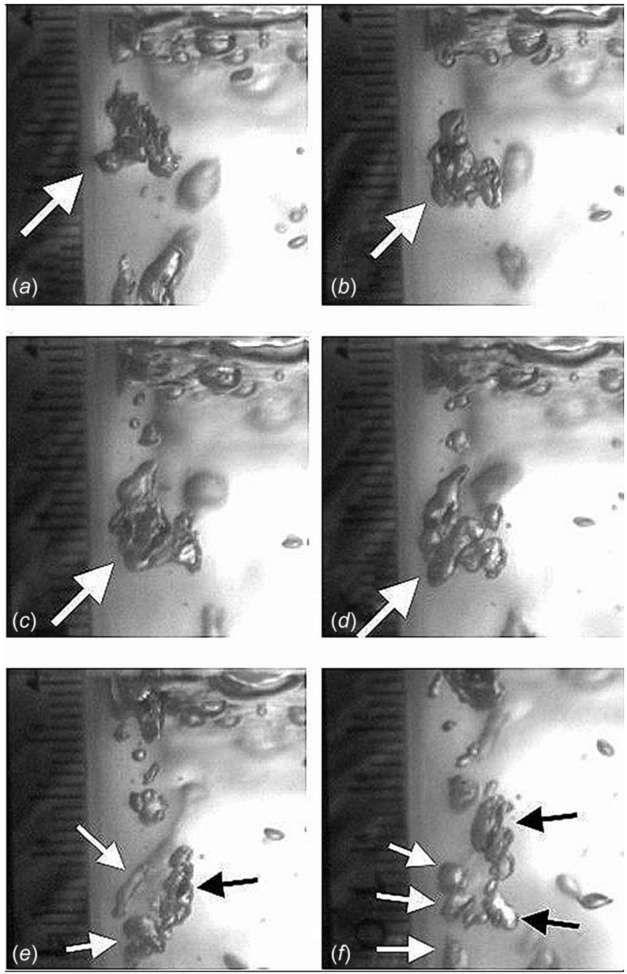

Fig. 6 Photographic sequence of explosion bubble breakup mechanism. Flow conditions: $V_1 = 1.26$ m/s, $x_1 = 0.05$ m. (1) Unstable bubble: (*a*) $t = 0.000$ s and (*b*) $t = 0.015$ s. (2) Explosion of the bubble: (*c*) $t = 0.024$ s and (*d*) $t = 0.031$ s. (3) Multiples daughters: (*e*) $t = 0.044$ s and (*f*) $t = 0.058$ s. Arrows indicating mother and daughter bubbles.

mechanism was relatively similar and appeared not to be influenced by the secondary breakups (Fig. 9(*b*)). The average size of the mother bubbles, characterized by the bubble two-dimensional cross-sectional area A, increased from $A = 72\ \text{mm}^2$ to $A = 96\ \text{mm}^2$ for entrained bubbles with primary breakup, when V_1 increased from 1.0 m/s to 1.26 m/s (Fig. 9(*c*)). One exception was the bubbles with small dejection mechanism. Such bubbles appeared to be slightly smaller with increasing impact velocity. However, note that only two dejection events were observed at $V_1 = 1.0$ m/s and the data might not be representative. The average vertical position of bubble breakup(s) generally increased with increasing impact velocity, although the dejection breakup mechanism seemed to follow another trend with an outstanding data point at $V_1 = 1.0$ m/s (Fig. 9(*d*)). For the dejection breakup mechanism, the mother bubble tended to breakup further away from the impingement point than for other breakup mechanisms. The secondary breakup data seemed not to influence the general trend.

In most cases, the stretching and dejection breakup mechanisms led to one mother bubble breaking into two daughter bubbles (stretching) or one mother and one daughter (dejection), independent of the impact velocity. For the explosion mechanism, the average number of daughter bubbles increased from 2.33 for $V_1 = 1.0$ m/s to 4.67 (primary breakup only) or 3.33 (secondary breakups) for $V_1 = 1.26$ m/s. In average, the number of daughter bubbles was about 2.2 for all mechanisms. In the studies of self-

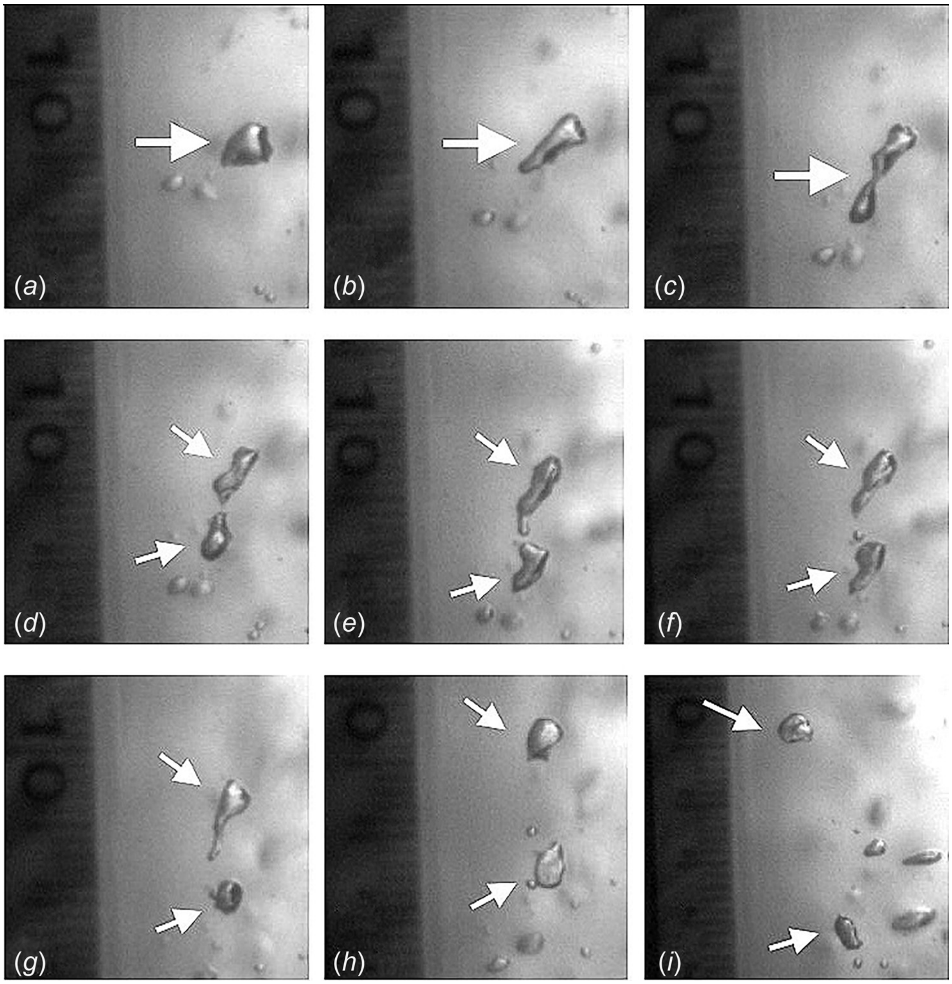

Fig. 7 Photographic sequence of stretching bubble breakup mechanism. Flow conditions: $V_1 = 1.26$ m/s, $x_1 = 0.05$ m. (1) Bubble stretching: (*a*) $t = 0.000$ s, (*b*) $t = 0.007$ s, and (*c*) $t = 0.012$ s. (2) Independent daughters: (*d*) $t = 0.015$ s, (*e*) $t = 0.020$ s, and (*f*) $t = 0.022$ s. (3) Daughters with different behaviors: (*g*) $t = 0.026$ s, (*h*) $t = 0.035$ s, and (*i*) $t = 0.077$ s. Arrows indicating mother and daughter bubbles.

aerated flows such as hydraulic jumps, plunging jets, spillway, and dropshaft flows, the breakup of entrained bubbles associated with the high turbulent shear forces was thought to be a main cause of the bubble clustering phenomenon [24,25]. Despite the variety of cluster definitions and the much higher air bubble concentrations, the majority of bubble clusters in these flows were found to be small clusters consisting of two bubbles, and the average number of bubbles per cluster was typically between 2 and 3 [26]. This was consistent with the present observations of a single breakup resulting in two daughter bubbles in most cases. It might imply that the fundamental bubble breakup mechanisms observed in the slightly aerated flow would likely persist in complex air–water flow environment with high turbulence levels.

6 Bubble Interplay and Coalescence

Qualitative observation showed that interactions between neighboring bubbles appeared more frequently than bubble breakup for $V_1 = 1.12$ and 1.26 m/s. A form of bubble interplay was bubble coalescence when two bubbles came into contact and merged into one. In most cases, bubbles formed by coalescence were unstable and experienced breakup later in their lifetime. Herein, the bubbles before coalescence are called parent bubbles, the bubbles resulting from the coalescence are called mother bubbles, and bubbles after the breakup of the mother bubble are called daughter bubbles. Typically, a bubble coalescence process may be divided into several stages, encompassing bubble approach, bubble contact/deformation, film drainage, and film rupture followed by air confluence [27,28]. Herein, the interacting parent bubbles were found to experience different stages, and overall four basic interaction behaviors were observed: (a) bubbles rebound, (b) bubble kiss-and-go, (c) bubble coalescence, and (d) collapse due to bubble interplay.

The first bubble interaction mechanism was the rebound mechanism, which typically included first the bubble attraction, followed by the bubble repulsion after rebound. In this mechanism, two bubbles were deemed to interact with each other without film rupture or any air exchange between the bubbles. Herein, rebound was considered when the bubble interaction influenced the shape and/or direction and/or velocity of the bubbles (Fig. 10). The parent bubbles did not form a mother bubble. Figure 10 shows two bubbles interacting with each other and influencing their shapes without any air exchange.

The second interaction behavior was described as kiss-and-go, during which two or more bubbles contacted and attached together for a duration slightly longer than an immediate rebound. The entire process consisted of the initial bubble attraction, the "kiss," followed by bubble repulsion, the "go." The optical observation could not identify whether there was any air exchange between the bubbles or not. A mother bubble may be considered to form temporarily from two (or more) parents; it had not a perfect shape and could clearly be seen as the result of the interactions between

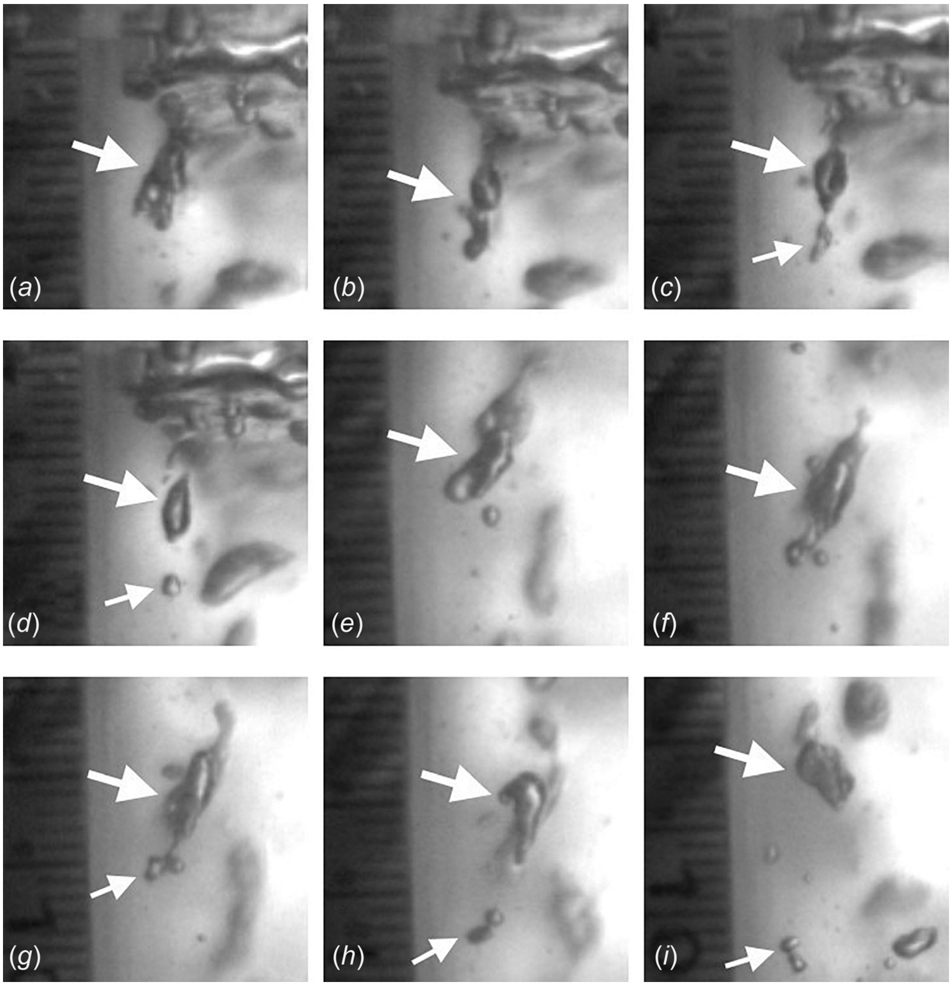

Fig. 8 Photographic sequence of dejection bubble breakup mechanism. Flow conditions: $V_1 = 1.26$ m/s, $x_1 = 0.05$ m. (1) First dejection: (*a*) $t = 0.000$ s, (*b*) $t = 0.004$ s, and (*c*) $t = 0.007$ s. (2) Mother and daughter independent behaviors: (*d*) $t = 0.012$ s and (*e*) $t = 0.036$ s. (3) Second dejection: (*f*) $t = 0.044$ s and (*g*) $t = 0.047$ s. (4) Mother and daughter independent behaviors: (*h*) $t = 0.051$ s and (*i*) $t = 0.064$ s. Arrows indicating mother and daughter bubbles.

two (or more) bubbles. After the "kiss," the two (or more) parents separated. The size of the mother bubble could be slightly different from that of the parent bubbles. Figures 11 and 12 show two examples of bubbles kissing events with some different attaching time durations, followed by a breakup or discharge behavior. In both examples, air exchange was considered unlikely to occur because the observed attaching time was much longer than the time required for film rupture between bubbles.

The coalescence mechanism was sometimes difficult to be distinguished from a kiss-and-go with the present lighting conditions. A true coalescence is typically accompanied by surface waves on the coalescing bubble surfaces associated with the release of large surface energy. This could not be clearly identified in the present videos from an instable bubble shape. The coalescence and formation of mother bubbles were usually followed by some subsequent breakup. The breakup mechanisms were the same as previously presented in Sec. 5.

The last typical bubble interplay was a collapse induced by the approaching of a neighbor bubbles. Basically, a bubble had a breakup behavior directly caused by the presence of and interactions with another parent bubble at a distance smaller than the radius of the parent bubbles. The bubble behavior was highly influenced by a close proximity of another bubble that might have generated by high-energetic turbulent eddies (Fig. 13). Unfortunately, this mechanism was only observed during qualitative observations and could not be quantified. There was no direct contact between bubbles, and the parent bubbles did not form a mother bubble. Figure 13 shows a bubble breaking up linked to the proximity of another bubble.

The total number of bubble interplay events observed for each impact velocity are: five for $V_1 = 1.00$ m/s, 24 for $V_1 = 1.12$ m/s and 33 for $V_1 = 1.26$ m/s. The results deriving from this relatively small data size, particularly for the smallest impact velocity, must be considered with care. Figure 14 presents some statistical properties of observed bubble coalescence as functions of the impact velocity, in dimensionless forms. The interplay count rate and proportion of bubbles subjected to interactions increased with increasing impact velocity (Fig. 14(*a*)). Among these interaction events, about 20% were seen with a true coalescence mechanism, while the majority was the kiss-and-go mechanism (Fig. 14(*b*)). The proportion of interplay behaviors was found to be independent of jet impact velocity. The average parent bubble cross-sectional area tended to increase with increasing impact velocity, showing no correlation with the interplay mechanism (Fig. 14(*c*)). The same general trend was observed for the mother bubble, of which the average cross-sectional area was approximately twice as large as the area of parent bubbles. The average vertical position of the occurrence of interaction/coalescence is presented in Fig. 14(*d*), and the up-pointing dash line originating from each data point represents the average longitudinal distance covered during bubble interplay. On average, bubbles with coalescent mechanism were observed to interact further away from the

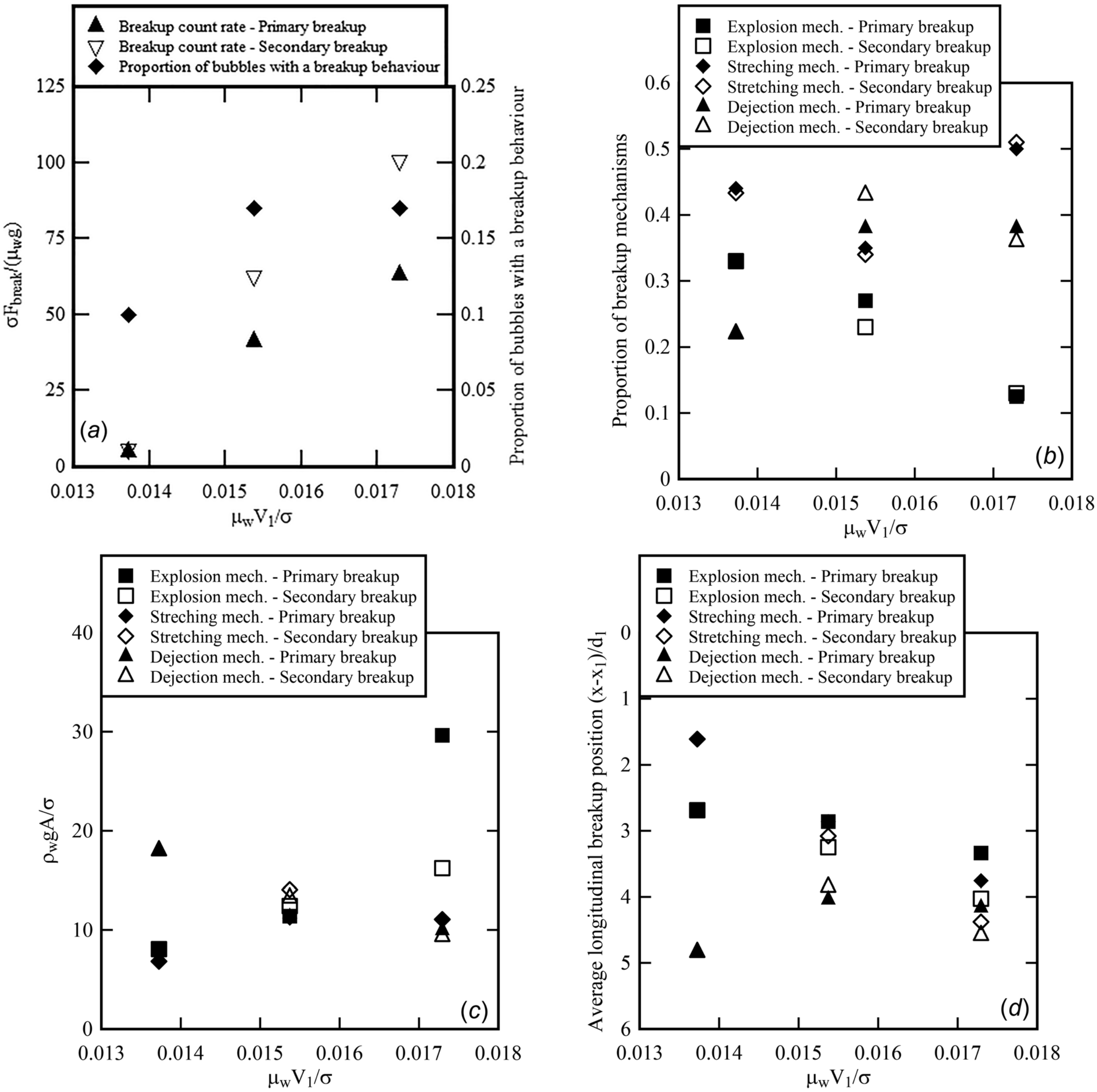

Fig. 9 Dimensionless statistical properties of bubble breakup events as functions of plunging jet's dimensionless impact velocity $\mu_w V_1/\sigma$: (*a*) bubble breakup count rate $\sigma F_{break}/(\mu_w g)$ and proportion of bubbles experiencing primary breakup, (*b*) proportion of different breakup mechanisms, (*c*) average cross-sectional area of mother bubbles $\rho_w gA/\sigma$, and (*d*) average vertical position of breakup $(x - x_1)/d_1$

impinging point. These bubbles also covered a larger distance than all other interaction mechanisms. The effects of the impact velocity were not obvious. In addition, these coalescing bubbles had a longer duration of interplay, which increased with increasing jet impact velocity.

The subsequent breakup mechanisms of coalescent bubbles were also investigated. Results are presented in Table 3. The breakup mechanisms were similar to those of individual bubbles (Sec. 5), except for the small dejection mechanism, which was not observed. The explosion mechanism seemed to be slightly more frequent than the stretching mechanism, although it could be also simply because of small sample size, and the average proportions for all three impact velocities were 56% (explosion) and 44% (stretching), respectively. With increasing jet impact velocity, the proportion of those mechanisms tended to become similar. The average number of successive breakup and the average number of daughter bubbles showed no correlation with the coalescent bubbles breakup mechanism. A higher impact velocity ($V_1 = 1.26$ m/s) tended to result in more than one successive breakup after coalescence, generating an average of 2.8 daughter bubbles, which was greater than for an individual bubble breakup (Sec. 5).

7 Discussion on Plunging Jet Instabilities: Impingement Point and Vortex Frequencies

The flow motion was stable and relative smooth for low impact velocities: 1.0 m/s $< V_1 <$ 1.36 m/s. A further increase in jet velocity led to development of unsteady flow features, such as vertical oscillations of impingement point and formation of large-scale vortical structures in the shear layer beneath the impingement point (Fig. 15(*a*)). The oscillations of impingement point were influenced by the air entrainment and detrainment, and the associated flow bulking. It changed instantaneously the jet length, hence the jet impact velocity. The large-scale vortices were highly aerated. The formation and downstream advection of the vortices enhanced the entrainment of large air packets and the bubble re-

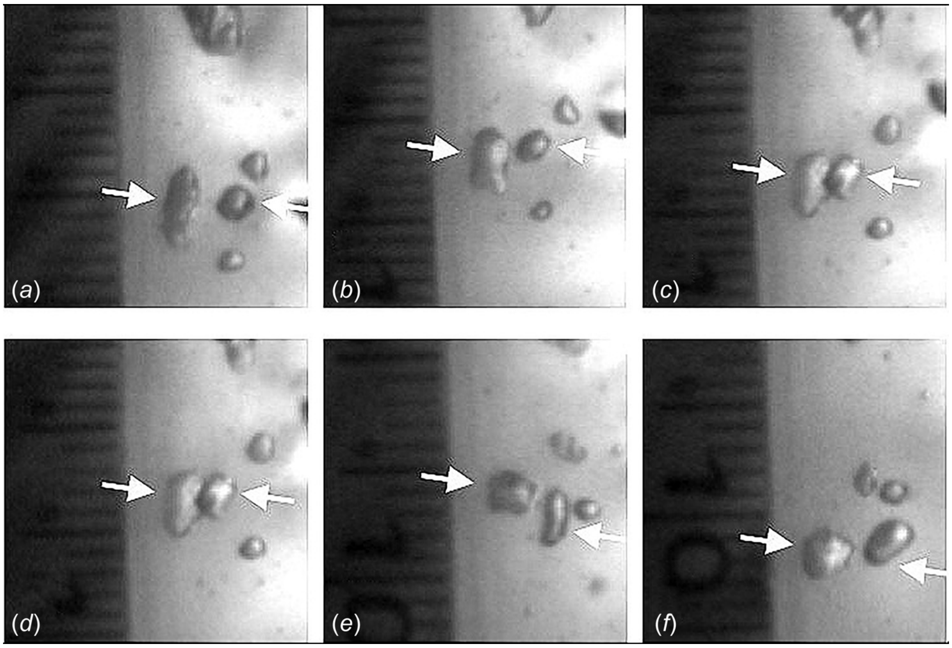

Fig. 10 Photographic sequence of rebound interplay mechanism. Flow conditions: $V_1 = 1.26$ m/s, $x_1 = 0.05$ m. (1) Bubble attraction: (*a*) $t = 0.000$ s, (*b*) $t = 0.005$ s, and (*c*) $t = 0.012$ s. (2) Bubble repulsion: (*d*) $t = 0.016$ s, (*e*) $t = 0.023$ s, and (*f*) $t = 0.038$ s. Arrows indicating parent bubbles.

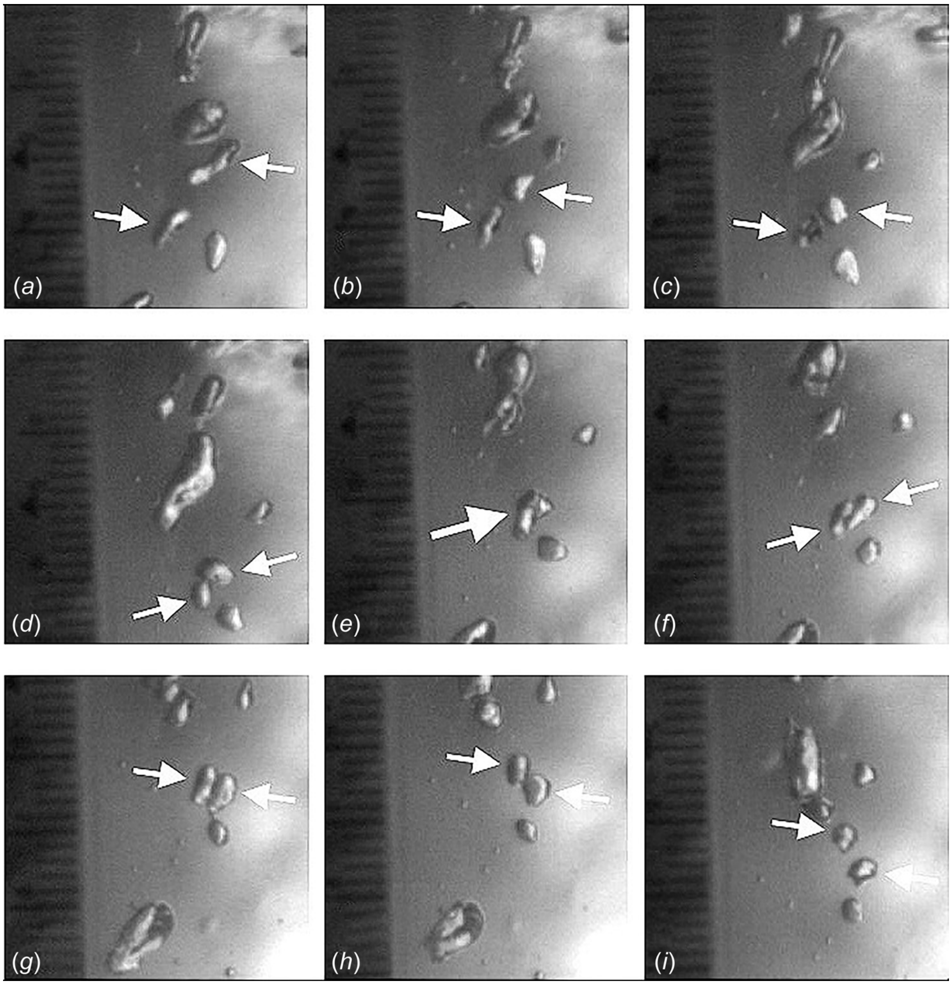

Fig. 11 Photographic sequence of "kiss-and-go" interplay mechanism. Flow conditions: $V_1 = 1.12$ m/s, $x_1 = 0.05$ m. (1) Bubble attraction: (*a*) $t = 0.000$ s, (*b*) $t = 0.005$ s, and (*c*) $t = 0.009$ s. (2) Bubble "kiss": (*d*) $t = 0.015$ s, (*e*) $t = 0.020$ s, and (*f*) $t = 0.025$ s. (3) Bubble repulsion: (*g*) $t = 0.031$ s, (*h*) $t = 0.035$ s, and (*i*) $t = 0.039$ s. Arrows indicating parent and mother bubbles.

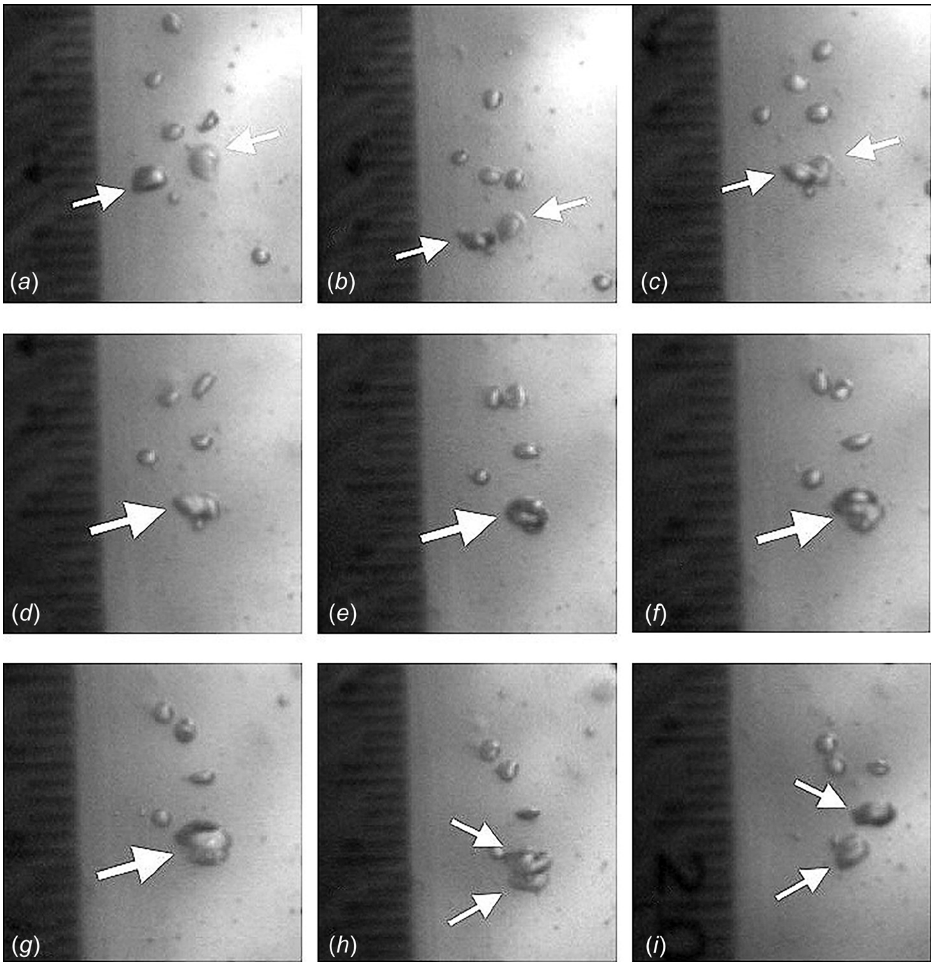

Fig. 12 Photographic sequence of "kiss-and-go" interplay mechanism. Flow conditions: $V_1 = 1.12$ m/s, $x_1 = 0.05$ m. (1) Bubble attraction: (*a*) $t = 0.000$ s, (*b*) $t = 0.016$ s, and (*c*) $t = 0.028$ s. (2) Bubble "kiss": (*d*) $t = 0.034$ s, (*e*) $t = 0.042$ s, (*f*) $t = 0.048$ s, and (*g*) $t = 0.053$ s. (3) Bubble repulsion: (*h*) $t = 0.058$ s and (*i*) $t = 0.086$ s. Arrows indicating parent, mother, and daughter bubbles.

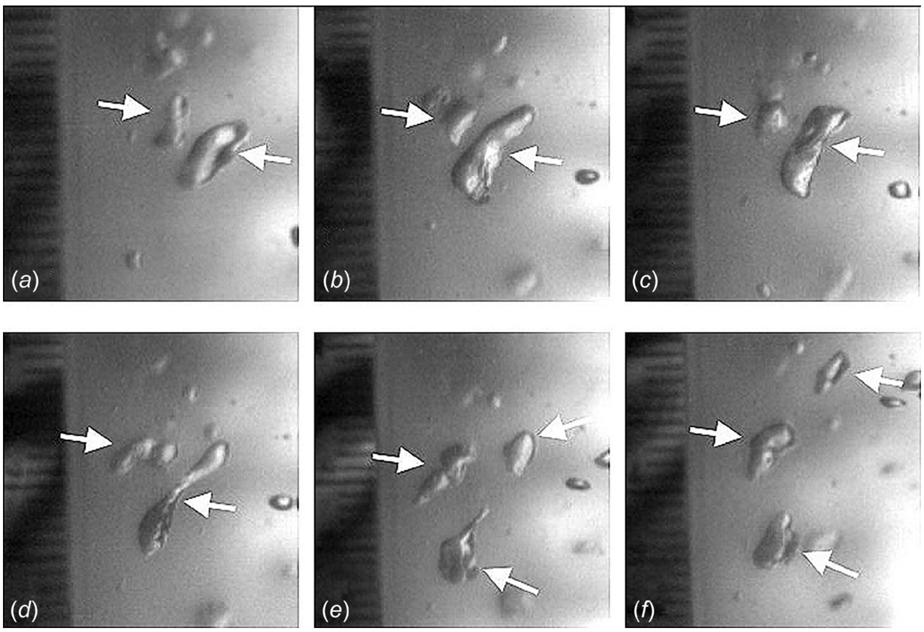

Fig. 13 Photographic sequence of collapse due to bubble approaching behavior. Flow conditions: $V_1 = 1.12$ m/s, $x_1 = 0.05$ m. (1) Stable bubble attraction: (*a*) $t = 0.000$ s, (*b*) $t = 0.010$ s, and (*c*) $t = 0.036$ s. (2) Bubble breakup: (*d*) $t = 0.042$ s, (*e*) $t = 0.050$ s, and (*f*) $t = 0.062$ s. Arrows indicating parent bubbles.

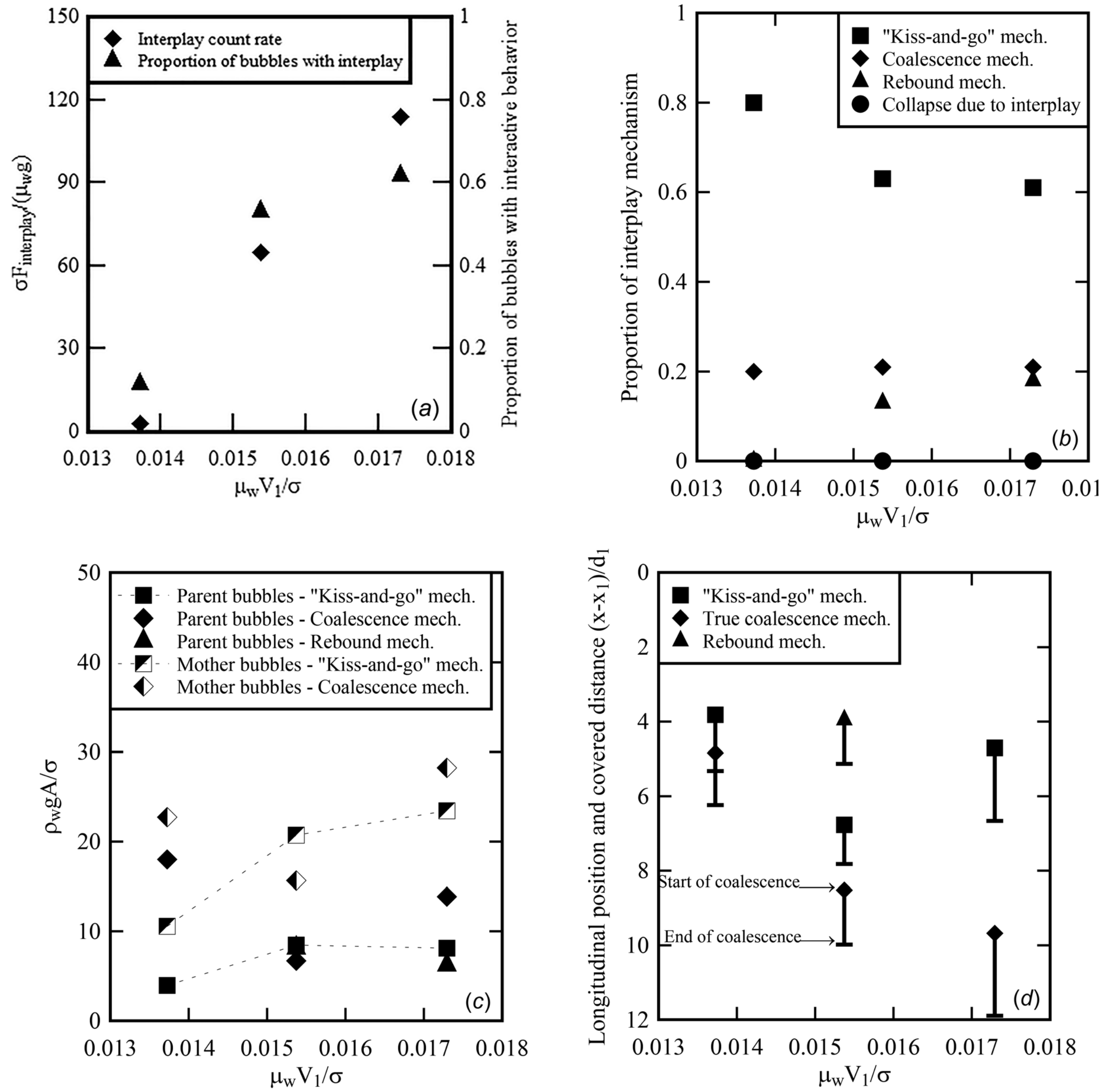

Fig. 14 Dimensionless statistical properties of bubble interplay events as functions of plunging jet's dimensionless impact velocity $\mu_w V_1/\sigma$: (a) bubble interplay count rate $\sigma F_{interplay}/(\mu_w g)$ and proportion of bubbles experiencing interplay, (b) proportion of different coalescence mechanisms, (c) cross-sectional area of parent bubbles and mother bubbles $\rho_w gA/\sigma$, and (d) average vertical position of occurrence of coalescence and average longitudinal distance covered during coalescence $(x - x_1)/d_1$

Table 3 Experimental observations of breakup of coalescent bubbles in plunging jets: the breakup mechanism, the average number of successive breakup of the mother bubble and the average number of daughter bubbles after breakup of a coalescent mother bubble

	Number of breakup bubbles			Average number of successive breakups		Average number of daughter bubbles	
Impact velocity, V_1 (m/s)	Explosion mech.	Stretching mech.	Dejection mech.	Explosion mech.	Stretching mech.	Explosion mech.	Stretching mech.
1.00	3	2	0	1.0	1.0	2.5	2.0
1.12	11	8	0	1.0	1.1	2.0	2.2
1.26	14	12	0	1.6	1.5	2.8	2.8

entrainment in the plunging pool. Such flow instabilities play a critical role in understanding bubble behaviors in high-speed plunging jets. Herein, a preliminary investigation of the characteristic frequencies of the oscillations of impingement point and the formation of aerated vortical structures is presented for a range of impact velocities 1.87 m/s $< V_1 <$ 4.24 m/s.

Both the impingement point oscillation and large vortex formation were observed in 600 fps. The video movies were analyzed

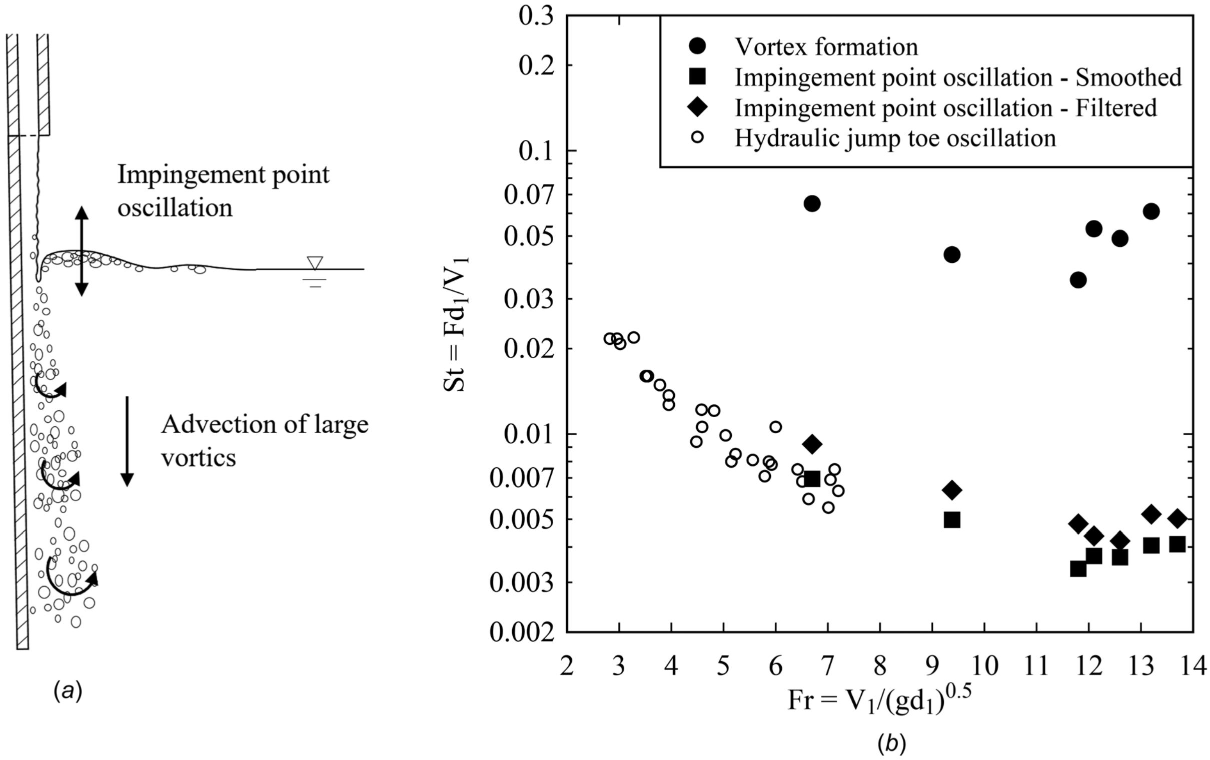

Fig. 15 Oscillation of impingement point and formation of large vortices in the plunging pool: (*a*) definition sketch and (*b*) dimensionless frequency data with comparison to observation of horizontal hydraulic jump toe oscillations by Wang and Chanson [29]

manually every 0.033 s (1 in 20 frames) for 30 s. The frequency of impingement point oscillations was derived from the time series of impingement point position that was either smoothed every ten points or filtered to eliminate high-frequency component over 20 Hz. The two approaches gave similar results (Fig. 15(*b*)), typically between 1.3 and 2.4 Hz and nearly independent of the jet impact velocity. The characteristic frequency of vortex formation and downstream ejection was found one order of magnitude greater, between 15 and 25 Hz. The Strouhal numbers of both frequencies are plotted in Fig. 15(*b*) as functions of the Froude number. The impingement point oscillation data are further compared with the observation of hydraulic jump toe oscillations by Wang and Chanson [29]. In hydraulic jumps, similar flow instabilities were noticed as shear layers form between the high-speed impinging flow and slower downstream water, although the direction of gravity was in perpendicular to the main flow direction. In spite of different ranges of the inflow Froude number, the data showed a consistent trend of decreasing Strouhal number with increasing Froude number. The magnitudes of the oscillations, on the other hand, were found to increase with increasing Froude number in both plunging jets and hydraulic jumps. The vortex observation in hydraulics jump was limited by the shutter speed of video camera and the results were not comparable to the present results.

8 Conclusion

Air bubble entrainment and the associated bubble breakup and interplay behavior were investigated in two-dimensional supported plunging jets at low impact velocities. That is, when the jet impact velocity was slightly greater than the critical onset velocity of air entrainment and individual bubble entrainment was visible. Several impinging jet flow patterns were investigated using a Phantom ultra-high-speed video camera with a frame rate up to 10,000 fps with full HD resolution.

The onset of air entrainment took place for an impact velocity $V_e = 0.9$ m/s to 1.1 m/s depending upon the free jet length. The data compared favorably with the literature in terms of the inception velocity V_e. At low impingement velocities from $V_1 = 1.0$–1.36 m/s, with $V_1 > V_e$, four individual mechanisms of air bubble entrainment were observed: single bubble entrapment, breakup of an elongated air cavity, air bubble pre-entrainment in the free jet, and bubble re-entrainment. While single bubbles constituted the majority of entrained air entities at onset of air entrainment, the formation and detachment of elongated air cavities became the predominant air entrainment mechanism for larger impact velocities. The single bubbles entrained at onset velocity had almost circular projection shapes at the entrapment point, and became slightly flatter after a vertical transport at an average velocity $V_b/V_1 \sim 0.46$.

The bubble breakup and interplay/coalescence processes were investigated both qualitatively and quantitatively. For $1.0 < V_1 < 1.26$ m/s, 10–17% of entrained individual bubbles broke. Three different breakup mechanisms were identified: explosion, split or stretching, and dejection. Interaction between bubbles was often observed for $V_1 = 1.12$ m/s and 1.26 m/s. Four interaction behaviors were observed: rebound, kiss-and-go, coalescence, and breakup due to bubble approaching. The coalescent bubbles were observed to be unstable and coalescence was often followed by a breakup mechanism. Overall, the increase in jet impact velocity complicated the entrained bubble behavior by enhancing the bubble breakup and interplay. Namely, with increasing impact velocity, more breakup and contact/coalescence events were observed within a given period of time, and the proportions of bubbles experiencing breakup and interplay increased significantly. An increase in impact velocity also led to larger average areas of mother bubbles before breakup and of parent bubbles before coalescence, as well as a longer longitudinal distance before the occurrence of breakup or contact. The average number of daughter bubbles resulting from the breakup of individual entrained bubbles increased slightly with increasing impact velocity, but this number was smaller than that of daughter bubbles resulting from successive breakups of unstable coalescent mother bubbles. With further larger impact velocities, the air entrainment started to interact with flow instabilities such as oscillations of impingement point and formation of large vortical structures in the shear flow.

Acknowledgment

The authors thank Dr. Frédéric Murzyn (ESTACA-Laval, France) for his comments on the project report and the technical assistance from Jason Van Der Gevel and Stewart Matthews (The University of Queensland) during the experiments.

Funding Data

- Australian Research Council (DP120100481).

References

[1] Bin, A., 1993, "Gas Entrainment by Plunging Liquid Jets," Chem. Eng. Sci., **48**(21), pp. 3585–3630.
[2] Chanson, H., 1997, *Air Bubble Entrainment in Free-Surface Turbulent Shear Flows*, Academic Press, London.
[3] Cummings, P. D., and Chanson, H., 1999, "An Experimental Study of Individual Air Bubble Entrainment at a Planar Plunging Jet," Chem. Eng. Res. Des., **77**(2), pp. 159–164.
[4] Kiger, K., and Duncan, J., 2012, "Air-Entrainment Mechanisms in Plunging Jets and Breaking Waves," Annu. Rev. Fluid Mech., **44**(1), pp. 563–596.
[5] Bertola, N., Wang, H., and Chanson, H., 2018, "A Physical Study of Air-Water Flow in Planar Plunging Water Jets With Large Inflow Disturbance," Int. J. Multiphase Flow, **100**, pp. 155–171.
[6] Mudde, R. F., 2005, "Gravity-Driven Bubbly Flows," Annu. Rev. Fluid Mech., **37**(1), pp. 393–423.
[7] Chanson, H., 2009, "Turbulent Air-Water Flows in Hydraulic Structures: Dynamic Similarity and Scale Effects," Environ. Fluid Mech., **9**(2), pp. 125–142.
[8] Ervine, D. A., McKeogh, E. J., and Elsawy, E. M., 1980, "Effect of Turbulence Intensity on the Rate of Air Entrainment by Plunging Water Jets," Proc. Inst. Civ. Eng., **69**(2), pp. 425–445.
[9] Risso, F., and Fabre, J., 1998, "Oscillations and Breakup of a Bubble Immersed in a Turbulent Field," J. Fluid Mech., **372**, pp. 323–355.
[10] Qian, D., MacLaughlin, J. B., Sankaranarayanan, K., Sundaresan, S., and Kontomaris, K., 2006, "Simulation of Bubble Breakup Dynamics in Homogeneous Turbulence," Chem. Eng. Commun., **193**(8), pp. 1038–1063.
[11] Ravelet, F., Colin, C., and Risso, F., 2011, "On the Dynamics and Breakup of a Bubble Rising in a Turbulent Flow," Phys. Fluids, **23**(10), p. 103301.
[12] Galinat, S., Risso, F., Masbernat, O., and Guiraud, P., 2007, "Dynamics of Drop Breakup in Inhomogeneous Turbulence at Various Volume Fractions," J. Fluid Mech., **578**, pp. 85–94.
[13] Orvalho, S., Ruzicka, M. C., Olivieri, G., and Marzocchella, A., 2015, "Bubble Coalescence: Effect of Bubble Approach Velocity and Liquid Viscosity," Chem. Eng. Sci., **134**, pp. 205–216.
[14] Del Castillo, L. A., Ohnishi, S., and Horn, R., 2011, "Inhibition of Bubble Coalescence: Effect of Salt Concentration and Speed of Approach," J. Colloid Interface Sci., **356**(1), pp. 316–324.
[15] Chesters, A. K., 1991, "The Modelling of Coalescence Processes in Fluid-Liquid Dispersions: A Review of Current Understanding," Chem. Eng. Res. Des., **69**(A4), pp. 259–270.
[16] Lasheras, J. C., Eastwood, C., Martinez-Bazán, C., and Montanes, J. L., 2002, "A Review of Statistical Models for the Break-Up of an Immiscible Fluid Immersed Into a Fully Developed Turbulent Flow," Int. J. Multiphase Flow, **28**(2), pp. 247–278.
[17] Revuelta, A., Rodriguez-Rodriguez, J., and Martinez-Bazan, C., 2006, "Bubble Break-Up in a Straining Flow at Finite Reynolds Numbers," J. Fluid Mech., **551**(1), pp. 175–184.
[18] Sanada, T., Sato, A., Shirota, M., and Watanabe, M., 2009, "Motion and Coalescence of a Pair of Bubbles Rising Side by Side," Chem. Eng. Sci., **64**(11), pp. 2659–2671.
[19] El-Hammoumi, M., 1994, "Entraînement d'Air par Jet Plongeant Vertical. Application aux Becs de Remplissage pour le Dosage Pondéral (Air Entrainment by Vertical Plunging Jet. Application to Refill Nozzles Applied to Dosage)," Ph.D. thesis, INPG, Grenoble, France (in French).
[20] Cummings, P. D., and Chanson, H., 1997, "Air Entrainment in the Developing Flow Region of Plunging Jets—Part 2: Experimental," ASME J. Fluids Eng., **119**(3), pp. 603–608.
[21] McKeogh, E. J., 1978, "A Study of Air Entrainment Using Plunging Water Jets," Ph.D. thesis, Queen's University of Belfast, Belfast, UK.
[22] Chirichella, D., Gomez Ledesma, R., Kiger, K., and Duncan, J., 2002, "Incipient Air Entrainment in a Translating Axisymmetric Plunging Laminar Jet," Phys. Fluids, **14**(2), pp. 781–790.
[23] Chanson, H., and Manasseh, R., 2003, "Air Entrainment Processes in a Circular Plunging Jet. Void Fraction and Acoustic Measurements," ASME J. Fluids Eng., **125**(5), pp. 910–921.
[24] Gualtieri, C., and Chanson, H., 2010, "Effect of Froude Number on Bubble Clustering in a Hydraulic Jump," J. Hydraul. Res., **48**(4), pp. 504–508.
[25] Gualtieri, C., and Chanson, H., 2013, "Interparticle Arrival Time Analysis of Bubble Distributions in a Dropshaft and Hydraulic Jump," J. Hydraul. Res., **51**(3), pp. 253–264.
[26] Wang, H., Hu, Z., and Chanson, H., 2015, "Two-Dimensional Bubble Clustering in Hydraulic Jumps," Exp. Therm. Fluid Sci., **68**, pp. 711–721.
[27] Li, D., 1996, "Coalescence Between Small Bubbles: Effects of Surface Tension Gradient and Surface Viscosities," J. Colloid Interface Sci., **181**(1), pp. 34–44.
[28] Kamp, A. M., Chesters, A. K., Colin, C., and Fabre, J., 2001, "Bubble Coalescence in Turbulent Flows: A Mechanistic Model for Turbulence-Induced Coalescence Applied to Microgravity Bubbly Pipe Flow," Int. J. Multiphase Flow, **27**(8), pp. 1363–1396.
[29] Wang, H., and Chanson, H., 2015, "Air Entrainment and Turbulent Fluctuations in Hydraulic Jumps," Urban Water J., **12**(6), pp. 502–518.